University of Baghdad
College of Engineering
JE
JOURNAL OF ENGINEERING

Journal of Engineering

journal homepage: www.jcoeng.edu.iq

Volume 32 Number 7 July 2026

Structure–Texture Relationships in Fe_3O_4/Deacetylated Chitin-Functionalized Mesoporous Silica Revealed by N_2 Adsorption–Desorption Isotherms

Tolin S. Othman [1,2], **Iqbal M. Mujtaba** [3], **Ammar S. Abbas** [1,*]

[1] Department of Chemical Engineering, College of Engineering, University of Baghdad, Baghdad, Iraq
[2] Department of Chemical Industries, College of Polytechnic-Kirkuk, University of Northern Technical, Kirkuk, Iraq
[3] Department of Chemical Engineering, School of Engineering, University of Bradford, Bradford BD7 1DP, UK

ABSTRACT

This work studied the textural properties of three adsorbents using nitrogen adsorption–desorption at a constant low temperature (77 K). The adsorbents are (a) mesoporous silica (MS), (b) mesoporous silica modified with Fe_3O_4 (MSF), and (c) mesoporous silica modified with Fe_3O_4 and coated with deacetylated chitin (MSFDAC). The adsorption–desorption isotherm curve demonstrated that the studied adsorbents have a mesoporous structure of type IV, according to the International Union of Pure and Applied Chemistry (IUPAC) classification. The obtained results show that the Brunauer–Emmett–Teller (BET) isotherm fits the data better than the Langmuir and the Freundlich isotherms. The surface area of MS was at its maximum value as compared to MSF and MSFDAC, which were 1000.55, 168.05, and 163.63 m^2/g, respectively. The analysis of particle size distribution for all adsorbent materials was in a narrow distribution, suggesting that the structures were mesoporous and well-defined. Despite slight variations in pore diameter distribution due to loading Fe_3O_4 and modification with deacetylated chitin, the MSFDAC adsorbent results in heterogeneity and unequal particle diameters. The average pore diameter increased from MS (4.6 nm) to MSF (7.32 nm) and MSFDAC (11.69 nm). Conversely, the total pore volume decreased from MS (1.15 cm^3/g) to MSF (0.89 cm^3/g) and MSFDAC (0.48 cm^3/g). A comparative study was carried out with the previous studies, which demonstrated that the textual properties of the modified magnetic silica adsorbent biomaterial agreed with those of other studies.

Keywords: Core-shell nanocomposites, Gas physisorption, Mesostructured evolution, Pore size distribution, Surface area modeling.

1. INTRODUCTION

Environmental pollution represents a persistent global challenge, driven by rapid industrial growth, urban expansion, and continuous technological development, resulting in significant

*Corresponding author
Peer review under the responsibility of University of Baghdad.
https://doi.org/10.31026/j.eng.2026.07.01

Article received: 09/05/2026
Article revised: 17/06/2026
Article accepted: 17/06/2026
Article published: 01/07/2026

risks to human health and ecological systems. Heavy metals such as lead (Pb), nickel (Ni), copper (Cu), mercury (Hg), and cadmium (Cd) are among the most important pollutants existing in water, which result from different industrial activities, and are characterized by high atomic weights and high densities **(Ali et al., 2021; Ghodke et al., 2021)**. Removal of pollutants according to development efficiency, economy, and environmentally friendly methods has become an immediate requirement **(Ali et al., 2021; Oladipo, 2018)**. Among the different techniques used for controlling pollution, adsorption has proved to be one of the most efficient and broadly used methods due to its high efficiency, simplicity in process, low cost, and ability to remove pollutants to low concentrations. Adsorption is a surface process in which adsorbent molecules accumulate on the surface of the adsorbent. Physical and chemical interactions between the adsorbate and the adsorbent surface control the process **(Ghodke et al., 2021; Kurji and Abbas, 2022; Minamisawa et al., 2004)**.

There are two main types of adsorption processes, which are physical adsorption and chemical adsorption. Weak van der Waals forces characterize physical adsorption and are normally reversible, with relatively low temperatures being used. Conversely, chemical adsorption is associated with a strong interaction between the adsorbate and the adsorbent surface, and it is mostly irreversible. Improving the performance of adsorbent materials and enabling their selection for appropriate applications requires improving the overall efficiency of the adsorption process **(Ugwu et al., 2020; Yu et al., 2023)**. The efficiency of adsorption is significantly based on the properties of the physicochemical adsorbent, including pore volume, surface area, pore size distribution, and surface functionality. As a result, extensive research has been conducted on the development of adsorbent materials with improved performance. Most adsorbents, such as activated carbon, zeolites, silica-based materials, and various nanostructured adsorbents, all of which have important potential in environmental treatment **(Lu et al., 2007; Moradpour et al., 2021; Wu et al., 2008)**. Among these materials, mesoporous materials are significant due to their structural properties. Mesoporous materials (MS) such as MCM-41, MCM-48, and SiO_2 are defined as materials having a pore diameter in the range of 2-50 nm, which provides a large surface area and allows the molecules to transfer into the internal structure **(Kurji and Abbas, 2022).** The characteristics of mesoporous silica materials are distinguished by their regular structure and uniform pore size, making them suitable for many applications **(Amin et al., 2023; Diez et al., 2015; Ezzeddine et al., 2025, 2023)**. In addition to mesoporous materials, magnetic nanoparticles such as Fe_3O_4 have been widely incorporated into adsorbent systems to enhance their functionality. Fe_3O_4 offers several advantages, including magnetic detachability, which facilitates recovery of the absorbent materials after the adsorption process using an external magnetic field to enhance their functionality **(Alattar et al., 2026; Wilczyńska et al., 2025)**

Furthermore, Fe_3O_4 can promote the interactivity between the adsorbent and contaminants, particularly heavy metal ions **(Jain, 2025; Zhang et al., 2020; Zhao et al., 2012)**. On the other hand, biopolymers have gained increasing advantages in the development of ecologically friendly adsorbents. Deacetylated chitin (DAC), a biopolymer material derivative from chitin, is one of the most promising biomass materials due to its non-toxic, biodegradable, and abundant functional groups such as hydroxyl (-OH) and amino ($-NH_3$) groups **(Rahman et al., 2019; Zhang et al., 2023)**. These functional groups supply active sites for adsorption and enhancement of the interaction with different pollutants. The use of DAC contributes to the sustainability of the material and improves adsorption properties **(Ali and Ali, 2024; Amin et al., 2023; Yu et al., 2020)**.

The combination of mesoporous materials, magnetic nanoparticles, and natural polymers has emerged as a promising strategy to achieve high performance **(Durán-Jiménez et al., 2019; Ragab et al., 2024)**. These hybrid materials aim to incorporate high surface areas and regular pore structure (mesoporous materials), magnetic properties (Fe_3O_4), and functional groups (natural materials like DAC) **(Ali et al., 2021; Quirarte-Escalante et al., 2009)**. Consequently, these compounds have the potential of offering better adsorption capacity, increased selectivity, and simple separation and regeneration **(Quirarte-Escalante et al., 2009; Samiey et al., 2014; Simsek et al., 2012; Song et al., 2022)**. The N_2 adsorption–desorption analysis is an essential method to describe the properties of surfaces and pores of adsorbent material and, thus, to assess adsorption behavior. The quantity of N_2 that gets attached to the adsorbent surface or within the pore space is proportional to the surface area of the adsorbent, the characteristics of the solid and gas, temperature, and the relative pressure of the gas **(Allache et al., 2025; Amrutha et al., 2023; Wang et al., 2025)**. Also, adsorption isotherms characterize both heterogeneous and homogeneous adsorption at the surface, which is the relationship between the quantity of N_2 adsorbed per unit mass of material and the relative pressure at a given temperature **(Calzaferri et al., 2023; Kurji and Abbas, 2022)**. According to the International Union of Pure and Applied Chemistry (IUPAC), adsorption behavior isotherms are identified by the shape of the isotherm curve and the type of hysteresis loop **(Al-Ghouti and Da'ana, 2020)**. The shape of the isotherm curve is classified into six categories; each type of shape describes a specific behavior of the adsorbent **(Kurji and Abbas, 2022)**. Isotherm models used to study adsorbent behavior are Langmuir, Freundlich, and Brunauer–Emmett Teller (BET) models. In addition to isotherm modeling, other methods may be used; the Barrett–Joyner–Halenda (BJH) and t-thickness methods are used to analyze pore- size distribution and the thickness (t) of the adsorbent layer. These models provide valuable information on the structural properties of the materials and their effects on adsorption behavior **(Saghapoor and Alizadeh, 2021)**.

Despite several studies **(Abukhadra et al., 2023; Alattar et al., 2026; Losito et al., 2021; Nasaj et al., 2022),** investigating mesoporous silica loaded with Fe_3O_4 and others investigating mesoporous silica modified with biopolymer materials, few studies have focused on the texture properties of each step in the modification of the mesoporous silica structure with Fe_3O_4 and biopolymer materials such as deacetylated chitin. The effects of changes at each step on N_2 adsorption-desorption behavior, hysteresis loops, surface area, average pore volume, and pore size distribution have not yet been fully understood.

The study aims to comparatively study the nature of the adsorption process and textural properties of MS, MSF, and MSFDAC. This study aimed to examine the textural properties of the studied materials by measuring nitrogen adsorption/desorption at 77 K, a standard temperature commonly used in physical nitrogen adsorption measurements due to the stability of nitrogen adsorption behavior at its boiling point. The experimental data obtained were interpreted using different adsorption isotherm models to evaluate the surface and pore properties of the materials, with the resulting parameters being systematically compared to those reported in previous studies.

2. EXPERIMENTAL AND THEORETICAL WORK

2.1 Adsorption–Desorption Tests

Nitrogen adsorption–desorption measurements were performed for MS, MSF, and MSFDAC samples at 77 K using a surface area analyzer (BET, BELSORP mini, Japan). The samples

studied were commercially supplied by Sigma-Aldrich (Germany) and used as received without any additional processing. Before analysis, the samples were conditioned to remove moisture and any weakly bound species, which could otherwise influence the adsorption behavior by drying them overnight at 85 °C. The N_2 adsorption–desorption measurements were conducted at the Petroleum Research and Development Center / Iraq. Each experiment was repeated twice to verify the consistency of the obtained data. The variation between repeated runs was minimal; therefore, the average values were adopted for further analysis. The obtained N_2 adsorption–desorption data were subsequently used to fit adsorption isotherms and to estimate key textural properties, including specific surface area, pore volume, and pore-size distribution. These parameters are directly relevant to interpreting the adsorption performance of the materials.

2.2 Langmuir Isotherm Model

One of the most popular models that is used to describe adsorption processes is the Langmuir isotherm model. It assumes that adsorption is taking place on a homogeneous surface, which occurs at a similar rate to a finite active site. At any given adsorption site, it can only fit one adsorbate molecule, and thus, the coverage by the adsorbate is monolayer, and there is no interaction between the adsorbed species **(Foo and Hameed, 2010)**. The linear form of the Langmuir model is represented in Eq. (1).

$$\frac{\mathrm{P}}{\mathrm{Q}_A} = \frac{\mathrm{P}}{\mathrm{Q}_{Am}} + \frac{1}{\mathrm{Q}_{Am}\mathrm{K}_L} \quad (1)$$

Where P represents the pressure (mmHg) at equilibrium, Q_A (cm^3/ g) is the volume of nitrogen that is adsorbed at a constant temperature and pressure, and Q_{Am} (cm^3/g) is the maximum monolayer adsorption on the solid surface. K_L can be related to the difference in the suitable area and adsorbent porosity, which indicates a higher adsorption capacity that can result in higher pore volume and surface area.

2.3 Freundlich Isotherm Model

The Freundlich isotherm model is an extensively applied model used to describe adsorption on heterogeneous surfaces. It assumes that the process of adsorption occurs on the surface with a non-regular distribution of the heat of adsorption. Freundlich isotherm model provides for multilayer adsorption and assumes that stronger linking sites are occupied first, followed by weaker sites as the adsorbate concentration increases. The linear form of the Freundlich model equation is represented in Eq. (2) **(Foo and Hameed, 2010)**.

$$\ln\mathrm{Q}_A = \ln\mathrm{K}_F + \frac{1}{n}\ln\mathrm{P} \quad (2)$$

Where K_F represents the Freundlich constant, which refers to adsorption capacity, and n (the adsorption intensity), which represents the strength or nature of the adsorption process, the favorability value of n is between 1 and 10, and when 1/n is less than 1, it represents homogenous adsorption.

2.4 BET Isotherm Model

The BET isotherm model is an essential method employed to analyze gas adsorption statements for the determination of the specific surface area of porous materials. The BET

theory includes the principle of multilayer adsorption on solid surfaces. The BET model assumes that adsorption takes place in multiple layers, where the preliminary layer is adsorbed with various energy compared to the subsequent layers, and the top layers act similarly to the condensation of the adsorbate **(Saghapoor and Alizadeh, 2021; Sugawara and Nikaido, 2014; Thommes, 2010)**. The linear form of the BET isotherm model is represented in Eq. (3).

$$\frac{\left(\frac{P}{P_o}\right)}{Q_A\left[1-\left(\frac{P}{P_o}\right)\right]} = \frac{(C-1)}{Q_{Am}C}\left(\frac{P}{P_o}\right) + \frac{1}{Q_{Am}C} \quad (3)$$

Where Q_A volume of nitrogen that is adsorbed at relative P/P_o, Q_{Am} is the maximum volume of nitrogen that is adsorbed on the solid surface to form a complete monolayer, P is the pressure equilibrium, P_o is the saturated pressure, and C is the BET constant, which is related to the adsorption energy. Only a limited range of relative pressures (0.05-0.3) allowed the BET equation to be used for the nitrogen adsorption data collected in this investigation.

2.5 Determination of the Total Surface Area

The total surface area (SA) of adsorbents was verified using Eq. (4) **(Thommes, 2010)**.

$$SA = \frac{NQ_{Am}A_{N2}}{V} \quad (4)$$

Where N is Avogadro's number, A_{N2} is the cross-sectional area of the N_2 molecule, which is equal to 0.162 nm^2, and V is the molar volume for the N_2 molecule, which equals 22.414 L/mole.

2.6 BJH Pore Diameter and Volume

BJH is a method utilized for determining the pore size diameter (d_{BJH}) and pore volume (V_p). This method can be calculated from experimental data by the N_2 adsorption–desorption isotherm at 77 K. BJH was enhanced in 1951 by considering that all pore structures are cylindrical, having open nonintersecting ends. According to Eq. (5), the BJH model assumed that the pore radius (r_p) was equal to the sum of the Kelvin radius and the thickness (t) of the adsorbed layer **(Medina-Rodriguez and Alvarado, 2021; Saghapoor and Alizadeh, 2021)**.

$$ln\left(\frac{P}{P_o}\right) = -\frac{2\gamma\upsilon\cos(\theta)}{RT(r_p - t)} \quad (5)$$

Where P/P_o is a relative pressure, γ is the liquid surface tension in (N/m), υ is the molar volume of the adsorbed, θ is the contact angle (assumed to be 0˚) between the adsorbate and adsorbent, R is the gas constant (8.314 J/K mole), T is the absolute temperature, and (r_p - t) represents the Kelvin radius.

2.8 Thickness of the Adsorbed Layer

The Halsey equation Eq. (6) provides a method to determine the thickness (t) of the adsorbent layer dropped on the pore walls **(Barrett et al., 1951).**

$$t = 3.54\left(\frac{-5}{ln\left(\frac{P}{P_o}\right)}\right)^{1/3} \quad (6)$$

3. RESULTS AND DISCUSSION

3.1 Adsorption–Desorption Isotherms

The N_2 adsorption–desorption data were used to identify the isotherm type and therefore the nature of the adsorption process for the selected adsorbent material. The N_2 adsorption–desorption isotherms were over the surface of the MS, MSF, MSFDAC as shown in **Fig. 1**. The adsorption curve from the adsorption–desorption isotherm clarifies the amount of N_2 molecules which adsorbent on surface of adsorbate and within the pores as the proportional pressure increases, while the desorption curve represents the removal of these molecules (N_2 molecules) with reduction of pressure as displayed in **Fig. 1**.

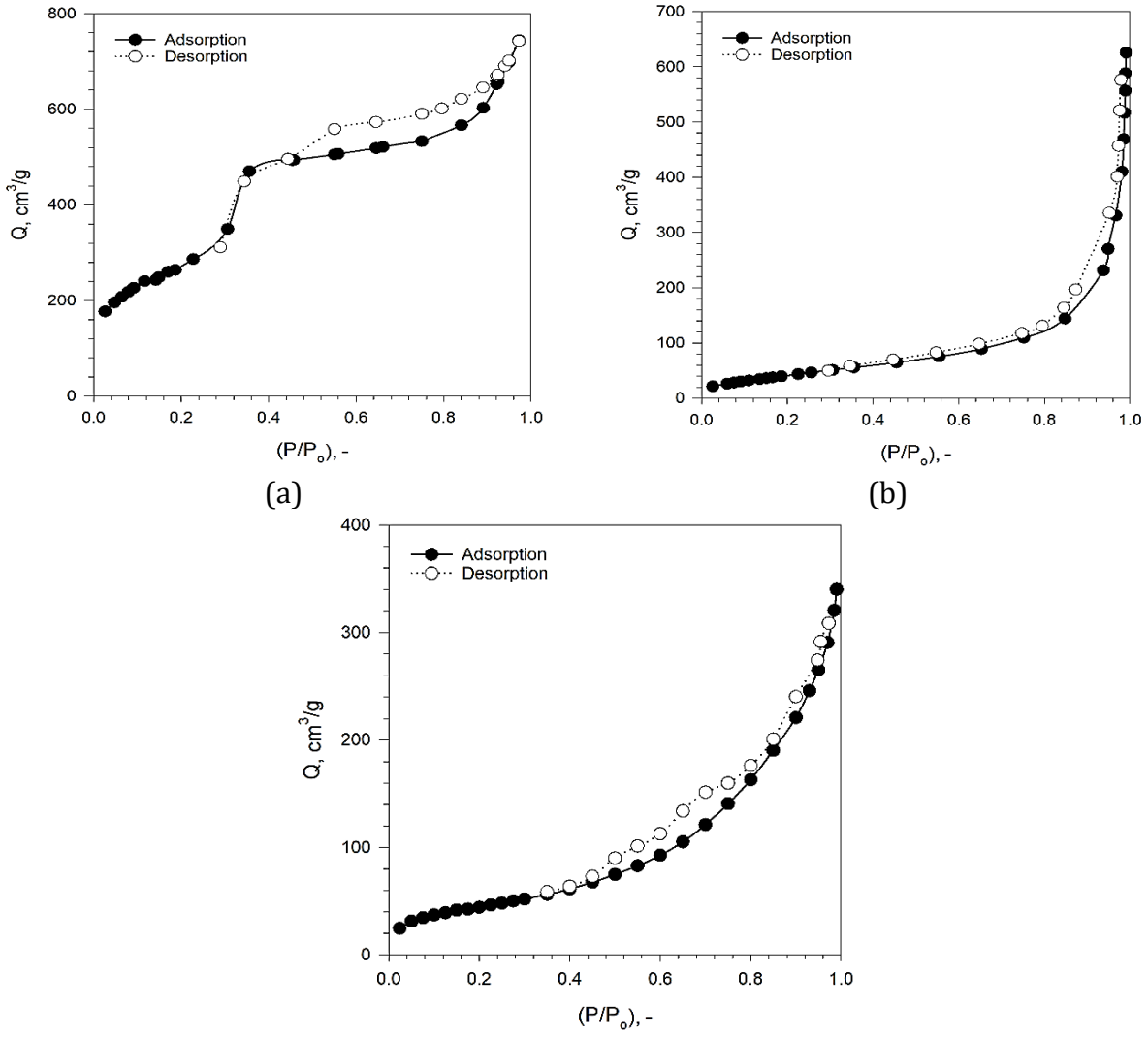

Figure 1. N_2 adsorption–desorption isotherm (a) MS (b) MSF (c) MSFDAC

The maximum amounts of N_2 adsorbed at P/P_o for the samples were 743 cm^3/g for MS. After uploading Fe_3O_4, the adsorption amount decreased to 625 cm^3/g for MSF because of surface covering and pore blocking by Fe_3O_4. The adsorption capacity of N_2 for the MSFDAC sample decreased to 350cm^3/g after modification by DAC. A decrease in the capacity of adsorption for MSFDAC is attributed to clear agglomeration by the DAC, which reduces the effect of capillary condensation and thus reduces the number of porous and specific surface areas. **Fig.1 (a)** shows the curve for MS initiates uptake at low relative pressure due to a strong interaction between the adsorbent - adsorbate and the presence of microporosity in the composition of silica. At intermediate pressure, about 0.3-0.4, the steep increase of adsorption capacity conforms to capillary condensation within the mesopores. The curve gradually went upwards with a nearly horizontal pass through a relative pressure of 0.4-0.8. The gradual upward trend refers to the fact that the filling of the pores is in multiple stages, which reflects that the distribution in pore size is wide and there is heterogeneity in the surface structure. After that, the curve rose sharply and continuously until the relative pressure reached 0.95. The desorption branch follows the adsorption branch in a parallel manner and closes the hysteresis loop at a relative pressure of 0.45, creating a distinct hysteresis loop. The hysteresis loop refers to characteristics of stability and mesoporous structure, with no pore blockage. The N_2 adsorption–desorption isotherm at 77 K can be classified as IV, and the behavior of the hysteresis loop is close to H2b type according to the IUPAC classification **(Do Nascimento et al., 2016)**.

In **Fig.1 (b)**, after being modified with Fe_3O_4, N_2 adsorption– desorption curves begin gradually with a steady rise from low relative pressure to 0.85 and are followed by a sharp rise with continuous rise until relative pressure reaches 0.99. The hysteresis loop is open and unsaturation, suggesting capillary condensation in slit-like pores usually noted in materials with layered or plate-like features. The structure is mesoporous and irregular in the distribution of pores, containing a void between the particles. According to the IUPAC classification, the type of curve is IV isotherm, and it corresponds to an H3-type hysteresis loop **(Thommes, 2010).** After modification with Fe_3O_4 and DAC, as shown in **Fig.1 (c)**, the curve closes the loop at P/P_o equal to 0.45 and continues with a gradual, unstable rise without apparent saturation until the relative pressure is close to one. According to IUPAC classification, the behavior of upward-opening shape without apparent saturation corresponds to a type IV isotherm with H3 hysteresis loop type **(Ramírez et al., 2005),** pointing out that the presence of mesoporous structures with either irregular or plate-like morphologies results from the accumulation of particles from DAC. The change in the hysteresis loop behavior reflects a progressive modification of the pore structure during loading with Fe_3O_4 and DAC coating. The MS material initially had a uniform pore structure. After the addition of Fe_3O_4 nanoparticles, the channels of pores in the structure of MS were partially filled with Fe_3O_4, creating spaces between the particles. The DAC coating increased the change in pore structure, creating more heterogeneity and less uniformity in the structure, with crack-like pores. The changes in pore structure are reflected in the curved shape, a reduction in surface area and pore volume, and an increase in pore radius, which refers to a gradual departure from the original silica's porous structure **(Kalam et al., 2021)**.

3.2 Adsorption–Desorption Isotherm Models

The Langmuir, Freundlich, and BET isotherm models were widely applied to interpret N_2 adsorption–desorption data obtained from porous materials, particularly for evaluating the textural characteristics. These models also provide a useful basis for identifying the most

representative adsorption description and estimating the adsorption capacity of the investigated different porous materials **(Erdogan, 2019; Kalam et al., 2021; Kurji and Abbas, 2022; Ladavos et al., 2012; Passe-Coutrin et al., 2008; Verma et al., 2024)**. Accordingly, the same modeling framework was employed in the present work to examine the textural properties of the synthesized porous materials, namely MS, MSF, and MSFDAC.

Fig. 2 shows the Langmuir isotherm model Eq. (1) for all three adsorbent materials. This isotherm model was fitted to the N_2 adsorption data for MS, MSF, and MSFDAC with coefficients of determination (R^2) equal to 0.9503, 0.9554, and 0.9879, respectively. Q_{Am} and K_L for all samples can be calculated from the slope and intercept of the linear plot, as shown in **Fig. 2** and reported in **Table 1**. The linear relation observed that R^2 for all adsorbent samples conformed to the Langmuir isotherm model, but not to a high degree **(Saghapoor and Alizadeh, 2021)**.

The Freundlich isotherm model for all materials, as shown in **Fig. 3**, was obtained from experimental data using the appropriate equation Eq. (2). The adsorption data yielded R^2 values of 0.9426 for MS and 0.958, 0.8525 for MSF and MSFDAC, respectively. The slope and intercept of the linearized model shown in **Fig. 3** can be calculated, and the resulting constants are reported in **Table 1**. These results indicate that the model is poor, suggesting that adsorption does not occur on a multilayer surface.

The experimental data points of the BET isotherm model Eq. (3) for three samples align closely with the nitrogen adsorption data presented in **Fig. 4**, emphasizing the mesoporous nature of the samples. All three samples presented the higher value of R^2, and higher adsorption capacity as in **Table 1**, when determined using the BET model, noting that this model is more accurate in representing the nitrogen adsorption behavior and the validity of the materials' mesoporous structure. The results for BET, as shown in **Fig. 4**, indicate that specific SA and pore volume of all adsorbents decreased in the same order.

The pure MS possesses a high SA_{BET} of about 1000.55 m^2/g because of the mesoporous structure, while the modified adsorbent samples introduced a reduction in SA_{BET} to about 168.05 m^2/g for MSF and 163.63 m^2/g for MSFDAC, because of pore blockage and structural modification. Additionally, the pore diameter remained within the mesoporous range (2–50 nm), confirming the conservation of mesoporous despite structural modification.

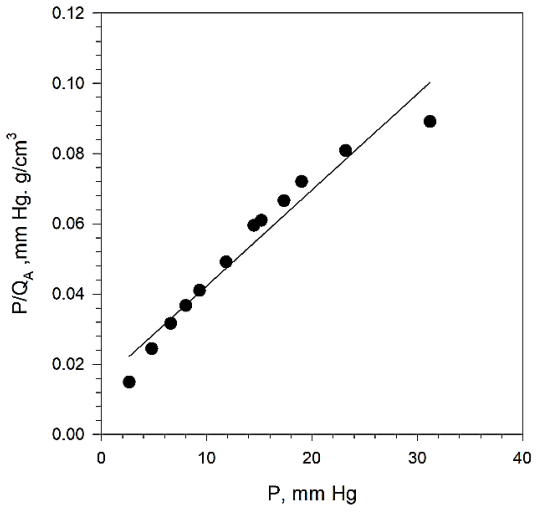

(a)

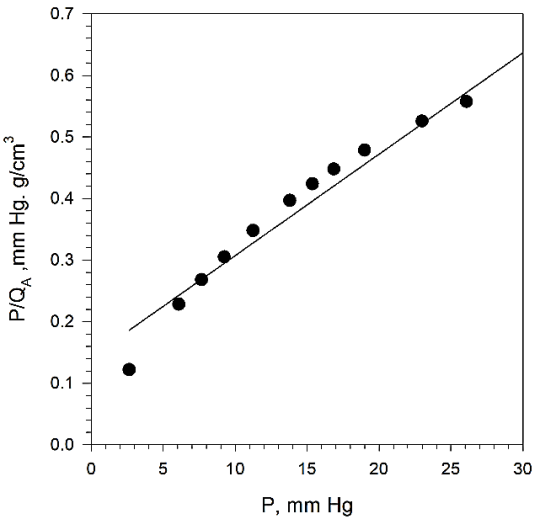

(b)

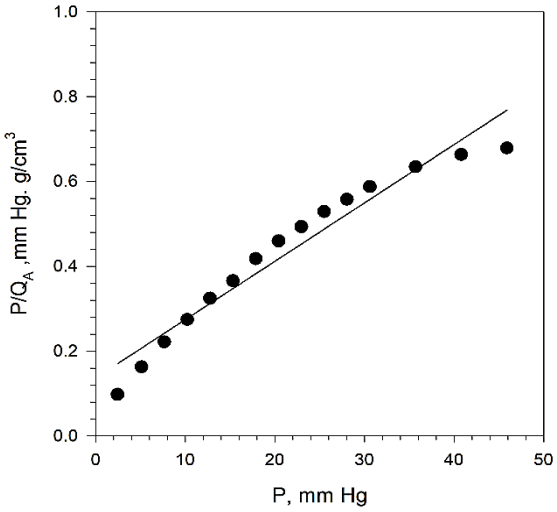

(c)

Figure 2. N_2 Adsorption Isotherm by the Langmuir Model (a) MS (b) MSF (c) MSFDAC

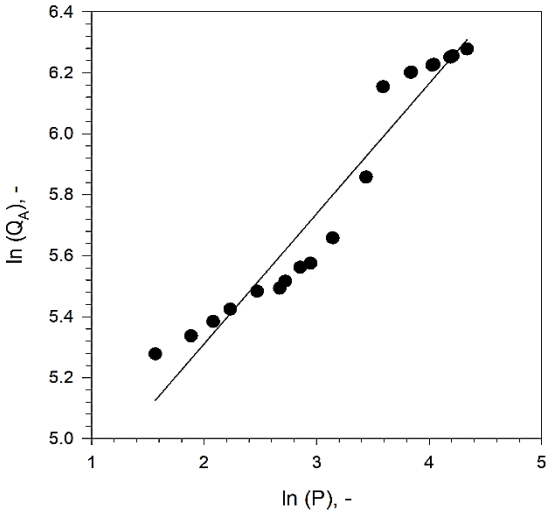

(a)

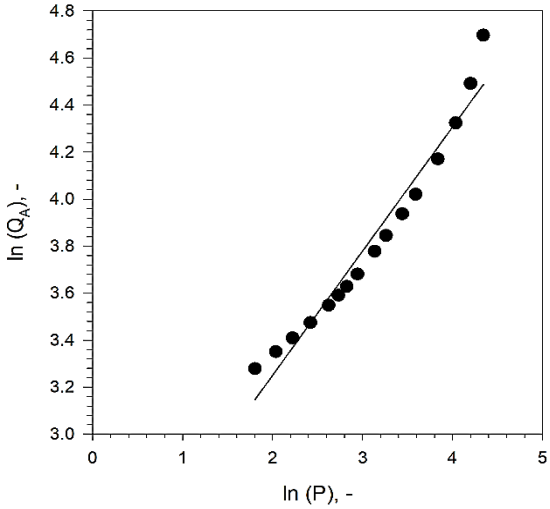

(b)

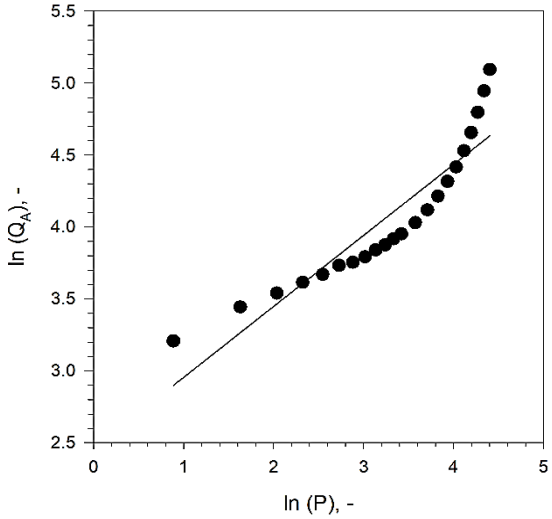

(c)

Figure 3. N_2 Adsorption Isotherm by the Freundlich Model (a) MS (b) MSF (c) MSFDAC

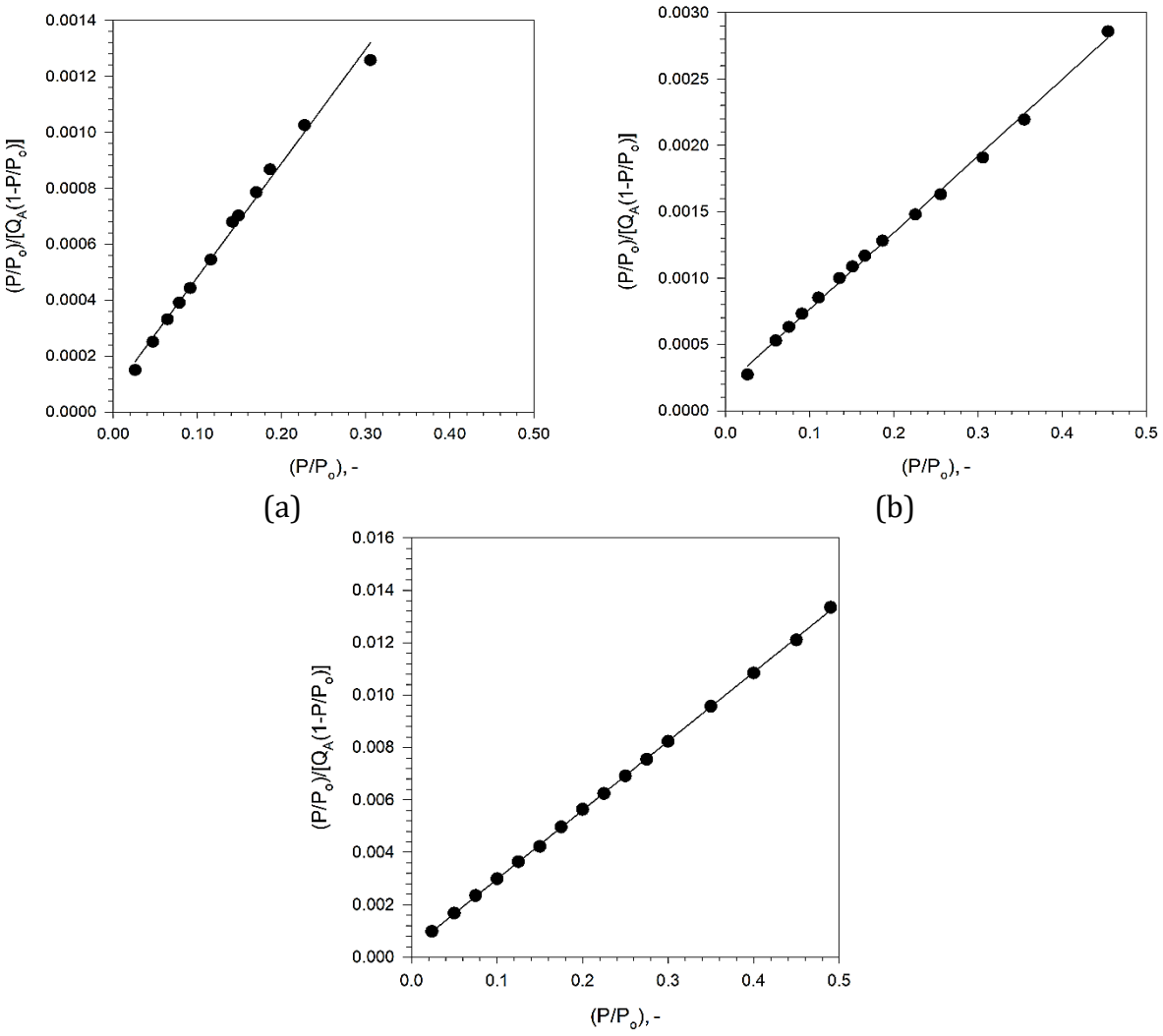

Figure 4. N_2 Adsorption Isotherm BET Model (a) MS (b) MSF (c) MSFDAC

Table 1. The Parameters and R^2 for the Isotherm Models

Isotherm model	parameters	MS	MSF	MSFDAC
Langmuir	$Q_{Am,}$ cm^3/g	66.67	7.00	11.38
	K_L, 1/mmHg	5.55	8.65	5.08
	R^2	0.9948	0.9554	0.9869
Freundlich	n	0.23	1.89	0.45
	K_f, $cm^3/g/(mmHg)^{(1/n)}$	1.10	158.49	3.58
	R^2	0.9426	0.9580	0.8525
BET	$Q_{Am,}$ cm^3/g	229.88	38.61	37.59
	C	1.01	1.04	1.02
	R^2	0.9991	0.9981	0.9998

3.3 Pore Size Distribution and Thickness of the Adsorbed Layer

Additionally, analysis of the pore size distribution in BJH (as shown in **Fig. 5**) and tabulated in **Table 2** detected that all samples MS, MSF, and MSFDAC have a mesoporous structure with a well-defined, moreover, narrow pore size distribution between 4 and 6.5 nm. For

modified adsorbent samples, a slight variation in the pore-size distribution suggests heterogeneity and the presence of pores of unequal sizes, likely due to Fe_3O_4 and DAC loading **(Do Nascimento et al., 2016)**. The calculated pore size diameters (as tabulated in **Table 2**) were 4.60 nm for MS, 7.32 nm, and 11.69 nm for MSF and MSFDAC, respectively. In a similar manner, the total pore volumes were 1.15 cm^3/g, 0.89 cm^3/g and 0.48 cm^3/g for each of MS, MSF, and MSFDAC, respectively. The t-plot analysis, as shown in **Fig. 6**, illustrates the relationship between t and Q_A for each adsorbent. For the MS sample (as shown in **Fig. 6 (a)**), the relationship is not linear; the curve steadily increases and then steeply increases, suggesting that adsorption occurs only on an external surface and that the pore is of the mesoporous type **(Allache et al., 2025; Song et al., 2022)**. In **Fig. 6 (b)** and **(c)** the relation increases in a semi-linear manner and deviates sharply upwards with increasing thickness. Suggesting that the adsorption is not restricted to the formation of surface layers but also includes partially blocked pores after loading of Fe_3O_4 and DAC. Thus, the analysis of the diagram confirms that the mesoporous structure is predominant with reduced uniformity after modification. Overall, the combination analysis of adsorption–desorption isotherms, BET SA, Langmuir modeling; BJH pore distribution, and t-plot indicates that while surface modification provides further functional properties and proves adsorption properties for pollutants, it simultaneously reduces the SA_{BET} and pore volume.

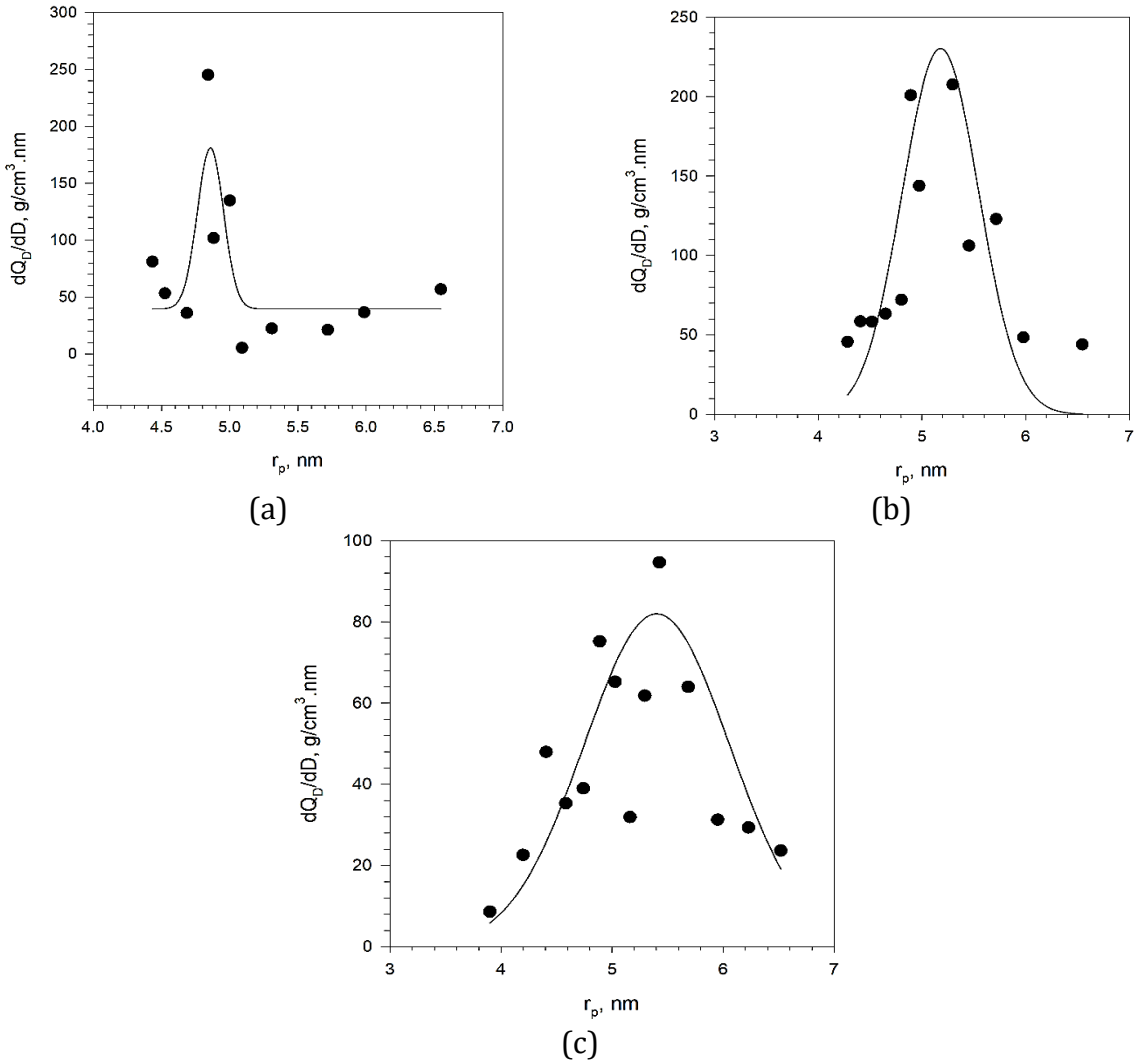

Figure 5. BJH particle size distribution for (a) MS (b) MSF (c) MSFDAC

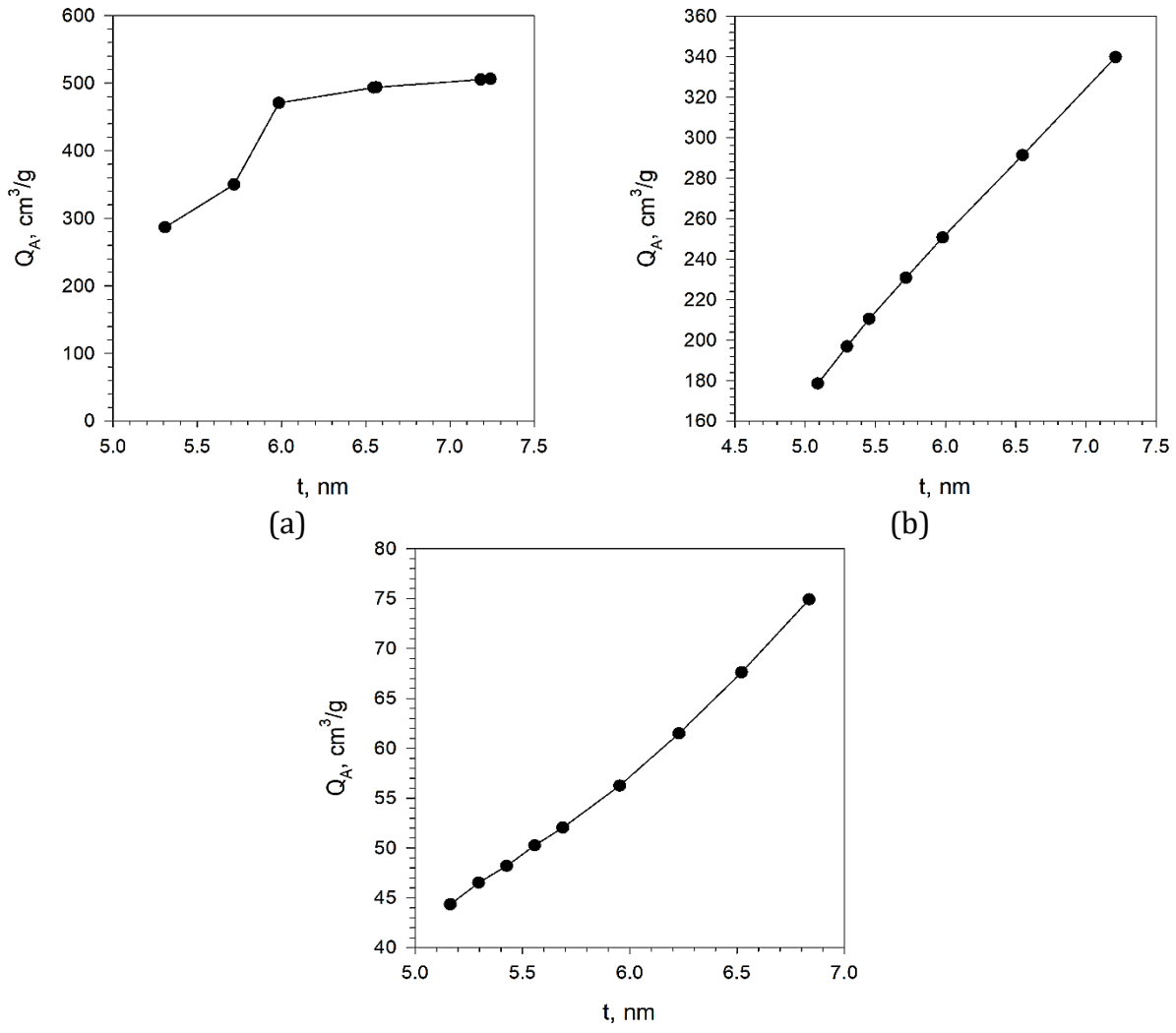

Figure 6. The t-plot for (a) MS (b) MSF (c) MSFDAC

3.4 Comparison of Surface Properties

A comparison of surface properties was summarized in **Table 2**, and a comparison was made with those advised for other adsorbents with porous structures in previous studies **(Do Nascimento et al., 2016; Guo et al., 2017; Muhammad Zakir Samriani et al., 2022; Zhang et al., 2024)**. The results became clear that the SA_{BET} and d_{BJH} of MS in the current study were in the range 809.90 - 1360.14 m^2/g for SA_{BET}, and in the range 3.04 - 4.9 nm for d_{BJH}, compared with these studies.

Moreover, the V_P of MS in the current study was higher or close to that of another mesoporous adsorbent, which ranged from 0.8 to 1.03 cm^3/g. However, upon modification with metal components and biopolymer materials compared with the current study, a decrease was observed in S_{BET} and pore volume as reported in **(Do Nascimento et al., 2016; Guo et al., 2017; Hatem et al., 2025; Samriani et al., 2022; Zhang et al., 2024)**.

In contrast, the study **(Hussein and Kareem, 2020)** reported that SA_{BET} and V_P increased after modification due to differences in the synthesis method. Fe_3O_4 was supported by a mesoporous material, which yielded results opposite those of other studies, as shown in **Table 2.** The decreases in the available SA_{BET} are commonly observed due to partial pore

blockage and structural modification **(Zhang et al., 2024)**. Similarly, the integration of materials such as DAC and other biopolymers can further influence the pore structure by covering active sites or introducing new functional groups **(Saad et al., 2005; Zhang et al., 2024)**.

Table 2. The Textural Characterization for Various Mesoporous Magnetic Adsorbents Found from N_2 Adsorption At 77 K

Adsorbent	SA_{BET} (m^2/g)	V_P (cm^3/g)	d_{BJH} (nm)	Reference
MS	1000.55	1.15	4.60	Current study
MSF	168.05	0.89	7.32	Current study
MSFDAC	163.63	0.48	11.69	Current study
MCM-48	1360.14	1.03	2.38	**(Kurji and Abbas, 2022)**
MCM-41	908.70	0.84	4.07	**(Do Nascimento et al., 2016)**
Ce-MCM-41	756.80	0.76	4.41	**(Do Nascimento et al., 2016)**
Fe_3O_4	54.14	0.23	15.33	**(Hussein and Kareem, 2020)**
Fe_3O_4@$mSiO_2$	1670.00	0.89	2.89	**(Hussein and Kareem, 2020)**
MCM-41@APTES	155.19	0.29	7.53	**(Hatem et al., 2025)**
MCM-41@APTES-BSAL	17.49	0.06	12.65	**(Hatem et al., 2025)**
MCM-41	920.43	0.80	3.04	**(Muhammad Zakir Samriani et al., 2022)**
Zn-MCM-41	896.04	0.78	2.94	**(Muhammad Zakir Samriani et al., 2022)**
MCM-41-A	809.9	0.97	4.9	**(Guo et al., 2017)**
CS-MCM-41-A	738.3	0.92	3.4	**(Guo et al., 2017)**
MCM-41	932.69	0.81	3.65	**(Zhang et al., 2024)**
0.16-Fe-MCM-41	350.28	0.64	2.67	**(Zhang et al., 2024)**

The modification with DAC and magnetic Fe_3O_4 reduces the overall adsorption capacity compared to pure MS. However, in the presence of functional groups that promote stronger chemical interactions and improved adsorption selectivity of pollutants such as heavy metals **(Abukhadra et al., 2023; Hatem et al., 2025; Wilczyńska et al., 2025)**. Additionally, the presence of magnetic properties, which contributes more easily to the separation and regeneration of the hybrid adsorbent after ending the adsorption process **(Kim et al., 2011; Zhao et al., 2012)**. Then, the modification of mesoporous materials makes the complex adsorbent more appropriate for targeted applications **(Parganiha and Patel, 2025; Ragab et al., 2024)**.

4. CONCLUSIONS

According to the IUPAC classification, the adsorption–desorption isotherm proves that the type of isotherm curve in each of MS, MSF, and MSFDAC is IV, which indicates that the structure of all materials has a mesoporous structure. The hysteresis loop of the MS sample is significant with type H2b, while the hysteresis loops for each MSF and MSFDAC sample are in H3 type. The linear relation and the higher value of R^2 in the BET isotherm model, which represents the suitable isotherm model for multi-layer N_2 adsorption behavior to the three selected materials, and is more accurate in surface area determination. The surface areas for MS, MSF, and MSDAC were 1000.55 m^2/g, 168.05 m^2/g, and 163.63 m^2/g, respectively. The BJH model, particle size distribution for three samples, has a well-defined

and narrow pore size distribution ranging from 4 to 6.5 nm. The pore size distributions of modified adsorbents showed slight variation, which indicates heterogeneity and the existence of pores of unequal sizes due to the loading of Fe_3O_4 and DAC. d_{BJH} for MS, MSF, and MSFDAC were 4.60 nm, 7.32 nm, and 11.69 nm, respectively, and V_P were 1.15, 0.89, and 0.48 cm^3/g for MS, MSF, and MSFDAC, respectively. The comparative results between the properties and those previously published for mesoporous materials indicated that there was a decrease in surface area and pore volume of modified mesoporous materials compared to pure mesoporous silica material. The observed changes in texture properties and increases in heterogeneity structure refer to the accessibility of adsorption active sites, which may affect the future absorption performance in practical applications for the modified materials.

NOMENCLATURE

Symbol	Description	Symbol	Description
A_{N2}	Cross-sectional area of N_2 molecules, nm^2	r_p	Pore diameter, nm
C	BET constant	R^2	Coefficient of determination, -
d_{BJH}	Pore size diameter, nm	R	Gas constant, J/K.mole
K_L	Langmuir constant,1/mmHg	SA	Total surface area, m^2/g
K_F	Freundlich constant, $cm^3/g/(mmHg)^{1/n}$	SA_{BET}	BET surface area, m^2/g
n	Favorability value	t	Thickness of adsorbed layer, nm
N	Avogadro number	T	Absolute temperature, K
P	Pressure equilibrium, mmHg	V	Molar volume of N_2, L/mole
P_o	Saturation pressure, mmHg	V_P	Pore volume, cm^3/g
P/P_o	Relative pressure, -	γ	Liquid surface tension, N/m
Q_A	Volume of N_2 adsorbed, cm^3/g	θ	Constant angle, degree
Q_{Am}	Maximum adsorption, cm^3/g	υ	Molar volume of adsorbed, cm^3/mole

Credit Authorship Contribution Statement

Tolin S. Othman: Methodology, Investigation, Formal analysis, Software, Data curation, Writing - original draft, Writing - review & editing. Iqbal M. Mujtaba: Supervision, Formal analysis, Validation, Writing - review & editing. Ammar S. Abbas: Conceptualization, Methodology, Formal analysis, Validation, Visualization, Writing - original draft, Writing - review & editing, Supervision, Project administration.

Declaration of Competing Interest

The authors declare that they have no known competing financial interests or personal relationships that could have appeared to influence the work reported in this paper.

REFERENCES

Abukhadra, M.R., Dardir, F.M., Ahmed, E.A., Soliman, M.F., Othman, S.I., Allam, A.A., Al Zoubi, W., Shaban, M.S., 2023. Insight into the Influence of the Integrated Chitosan on the Adsorption Properties of Chitosan/Al-MCM-41 Composite for As (V) Metal Ions: Characterization and Advanced Equilibrium Studies. *Nanomaterials and Nanotechnology*, pp. 1-16. https://doi.org/10.1155/2023/9879371

Alattar, R.A., Mihsen, H.H., Ahmed, L.M., 2026. Synthesis, characterization, and application of magnetic mesoporous MCM-41-Fe_3O_4 core-shell nanoparticles in the removal of Eosin Yellow Dye. *Indonesian Journal of Chemistry,* pp. 422–437. https://doi.org/10.22146/ijc.108056

Al-Ghouti, M.A., Da'ana, D.A., 2020. Guidelines for the use and interpretation of adsorption isotherm models: A review. *Journal of Hazardous Materials,* 393, P. 122383. https://doi.org/10.1016/j.jhazmat.2020.122383

Ali, D.A., Ali, R.G., 2024. Green synthesis of Carbonized Chitosan-Fe_3O_4-SiO_2 nano-composite for adsorption of heavy metals from aqueous solutions. *BMC Chemistry,* 18, P. 147. https://doi.org/10.1186/s13065-024-01257-5

Ali, N., Hassan Riead, M.M., Bilal, M., Yang, Y., Khan, A., Ali, F., Karim, S., Zhou, C., Wenjie, Y., Sher, F., Iqbal, H.M.N., 2021. Adsorptive remediation of environmental pollutants using magnetic hybrid materials as platform adsorbents. *Chemosphere*, 284, P. 131279. https://doi.org/10.1016/j.chemosphere.2021.131279

Allache, M., Cui, Y.J., Mokni, N., 2025. On the determination of pore size distribution by nitrogen Adsorption and Mercury intrusion Porosimetry for claystone, *E3S Web of Conferences,* 642, P. 03026. https://doi.org/10.1051/e3sconf/202564203026

Amin, K.F., Gulshan, F., Asrafuzzaman, F.N.U., Das, H., Rashid, R., Manjura Hoque, S., 2023. Synthesis of mesoporous silica and chitosan-coated magnetite nanoparticles for heavy metal adsorption from wastewater. *Environmental Nanotechnology, Monitoring and Management,* 20, P. 100801. https://doi.org/10.1016/j.enmm.2023.100801

Amrutha, Jeppu, G., Girish, C.R., Prabhu, B., Mayer, K., 2023. Multi-component Adsorption Isotherms: Review and Modeling Studies. *Environmental Processes,* 10, 38. https://doi.org/10.1007/s40710-023-00631-0

Barrett, E.P., Joyner, L.G., Halenda, P.P., 1951. The Determination of Pore Volume and Area Distributions in Porous Substances. I. Computations from Nitrogen Isotherms. *Journal of the American Chemical Society,* 73, pp. 373–380. https://doi.org/doi:10.1021/ja01145a126

Calzaferri, G., Gallagher, S.H., Lustenberger, S., Walther, F., Brühwiler, D., 2023. Multiple equilibria description of type H1 hysteresis in gas sorption isotherms of mesoporous materials. *Materials Chemistry and Physics,* 296, P. 127121. https://doi.org/10.1016/j.matchemphys.2022.127121

Diez, A.S., Alvarez, M., Volpe, M.A., 2015. Metal-modified mesoporous silicate (MCM-41) material: Preparation, characterization and applications as an adsorbent. *Journal of the Brazilian Chemical Society,* 26, pp. 1542–1550. https://doi.org/10.5935/0103-5053.20150122

Do Nascimento, G.E., Duarte, M.M.M.B., Barbosa, C.M.B.M., 2016. Cerium incorporated into a mesoporous molecular sieve (MCM-41). *Brazilian Journal of Chemical Engineering,* 33, pp. 541–547. https://doi.org/10.1590/0104-6632.20160333s20150132

Durán-Jiménez, G., Hernández-Montoya, V., Rodríguez Oyarzun, J., Montes-Morán, M.Á., Binner, E., 2019. Pb(II) removal using carbon adsorbents prepared by hybrid heating system: Understanding the microwave heating by dielectric characterization and numerical simulation. *Journal of Molecular Liquids,* 277, pp. 663–671. https://doi.org/10.1016/j.molliq.2018.12.143

Erdogan, F.O., 2019. Freundlich, Langmuir, Temkin, DR and Harkins-Jura isotherm studies on the adsorption of CO2 on various porous adsorbents. *International Journal of Chemical Reactor Engineering,* 17, P. 20180134. https://doi.org/10.1515/ijcre-2018-0134

Ezzeddine, Z., Batonneau-Gener, I., Ghssein, G., Pouilloux, Y., 2025. Recent Advances in Heavy Metal Adsorption via Organically Modified Mesoporous Silica: A Review. *Water,* 17, P. 669. https://doi.org/10.3390/w17050669

Ezzeddine, Z., Batonneau-Gener, I., Pouilloux, Y., 2023. Zinc Removal from Water via EDTA-Modified Mesoporous SBA-16 and SBA-15. *Toxics,* 11, P. 205. https://doi.org/10.3390/toxics11030205

Foo, K.Y., Hameed, B.H., 2010. Insights into the modeling of adsorption isotherm systems. *Chemical Engineering Journal*, 156, pp. 2–10. https://doi.org/10.1016/j.cej.2009.09.013

Ghodke, S.A., Maheshwari, U., Gupta, S., Sonawane, S.H., Bhanvase, B.A., 2021. Nanomaterials for adsorption of pollutants and heavy metals: Introduction, mechanism, and challenges, *Handbook of Nanomaterials for Wastewater Treatment: Fundamentals and Scale up Issues.* Elsevier, pp. 343–366. https://doi.org/10.1016/B978-0-12-821496-1.00032-5

Guo, Yige, Liu, D., Zhao, Y., Gong, B., Guo, Yujie, Huang, W., 2017. Synthesis of chitosan-functionalized MCM-41-A and its performance in Pb(II) removal from synthetic water. *Journal of the Taiwan Institute of Chemical Engineers,* 71, pp. 537–545. https://doi.org/10.1016/j.jtice.2016.12.033

Hatem, R.S., Mihsen, H.H., Hussain, A.F., 2025. Preparation of Novel Adsorbents via Functionalized MCM-41 Prepared from Plant Residues. *Baghdad Science Journal,* 22 (5). https://doi.org/10.21123/bsj.2024.10361

Hussein, E.A., Kareem, S.H., 2020. Magnetic mesoporous silica material (Fe_3O_4@$mSiO_2$) as adsorbent and delivery system for ciprofloxacin drug. *IOP Conference Series: Materials Science and Engineering. Institute of Physics Publishing,* 871, P. 012020. https://doi.org/10.1088/1757-899X/871/1/012020

Jain, R., 2025. Magnetite–graphene nanocomposites to treat contaminated water: a review. Appl. Water Sci. 15, 223. https://doi.org/10.1007/s13201-025-02486-2

Kalam, S., Abu-Khamsin, S.A., Kamal, M.S., Patil, S., 2021. Surfactant Adsorption Isotherms: A Review. *ACS Omega,* 6, pp. 32342–32348. https://doi.org/10.1021/acsomega.1c04661

Kim, B.C., Lee, J., Um, W., Kim, Jaeyun, Joo, J., Lee, J.H., Kwak, J.H., Kim, J.H., Lee, C., Lee, H., Addleman, R.S., Hyeon, T., Gu, M.B., Kim, Jungbae, 2011. Magnetic mesoporous materials for removal of environmental wastes. *Journal of Hazardous Materials,* 192, pp. 1140–1147. https://doi.org/10.1016/j.jhazmat.2011.06.022

Kurji, B.M., Abbas, A.S., 2022. Comparative Study of Textural Properties for Various Silica by Nitrogen Adsorption-desorption Technique. *Egyptian Journal of Chemistry*, 65, pp. 313–320. https://doi.org/10.21608/EJCHEM.2022.125169.5568

Ladavos, A.K., Katsoulidis, A.P., Iosifidis, A., Triantafyllidis, K.S., Pinnavaia, T.J., Pomonis, P.J., 2012. The BET equation, the inflection points of N_2 adsorption isotherms and the estimation of specific surface area of porous solids. *Microporous and Mesoporous Materials*, 151, pp. 126–133. https://doi.org/10.1016/j.micromeso.2011.11.005

Losito, D.W., de Araujo, D.R., Bezzon, V.D.N., Oseliero Filho, P.L., Fonseca, F.L.A., Chagas, C. dos S., Barbosa, E., Oliveira, C.L.P., Fantini, M.C. de A., Ferreira, F.F., Martins, T. da S., Haddad, P.S., 2021. Mesoporous Silica–Fe3O4 Nanoparticle Composites as Potential Drug Carriers. *ACS Applied Nano Materials,* 4, pp. 13363–13378. https://doi.org/10.1021/acsanm.1c02861

Lu, A.H., Salabas, E.L., Schüth, F., 2007. Magnetic nanoparticles: Synthesis, protection, functionalization, and application. *Angewandte Chemie International Edition*, 46, pp. 1222–1244. https://doi.org/10.1002/anie.200602866

Medina-Rodriguez, Bryan.X., Alvarado, Vladimir., 2021. Use of gas adsorption and inversion methods for shale pore structure characterization. *Energies,* 14, P. 2880. https://doi.org/10.3390/en14102880

Minamisawa, M., Minamisawa, H., Yoshida, S., Takai, N., 2004. Adsorption behavior of heavy metals on biomaterials. *Journal of Agricultural and Food Chemistry*, 52, pp. 5606–5611. https://doi.org/10.1021/jf0496402

Moradpour, N., Sedaghat, S., Aberoomand Azar, P., Behzad, K., 2021. Synthesis of chitosan and amine functionalized MCM-41 nanocomposite for the removal of acetylsalicylic acid from water using central composite design. *Applied Organometallic Chemistry*, 35 (8). https://doi.org/10.1002/aoc.6277

Muhammad Zakir, S., Taba, P., Nafie, N. La, Indriani, I., 2022. Synthesis of MCM-41 Silica Mesoporous Modified with Zn Metal. *Jurnal Kimia Sains dan Aplikasi*, 25 (8), pp. 286–291. https://doi.org/10.14710/jksa.25.8.286-291

Nasaj, M., Farmany, A., Shokoohizadeh, L., Jalilian, F.A., Mahjoub, R., Roshanaei, G., Nourian, A., Shayesteh, O.H., Arabestani, M.R., 2022. Development of Chitosan-Assisted Fe_3O_4@SiO_2 Magnetic Nanostructures Functionalized with Nisin as a Topical Combating System against Vancomycin-Intermediate Staphylococcus aureus (VISA) Skin Wound Infection in Mice. *Journal of Nanomaterials*, 2022. https://doi.org/10.1155/2022/2914210

Oladipo, A.A., 2018. Microwave-assisted synthesis of high-performance polymer-based nanoadsorbents for pollution control, *New Polymer Nanocomposites for Environmental Remediation. Elsevier Inc.*, pp. 337–359. https://doi.org/10.1016/B978-0-12-811033-1.00014-7

Passe-Coutrin, N., Altenor, S., Cossement, D., Jean-Marius, C., Gaspard, S., 2008. Comparison of parameters calculated from the BET and Freundlich isotherms obtained by nitrogen adsorption on activated carbons: A new method for calculating the specific surface area. *Microporous and Mesoporous Materials*, 111, pp. 517–522. https://doi.org/10.1016/j.micromeso.2007.08.032

Quirarte-Escalante, C.A., Soto, V., De La Cruz, W., Porras, G.R., Manríquez, R., Gomez-Salazar, S., 2009. Synthesis of hybrid adsorbents combining sol-gel processing and molecular imprinting applied to lead removal from aqueous streams. *Chemistry of Materials*, 21, pp. 1439–1450. https://doi.org/10.1021/cm801480v

Ragab, A.H., Mubarak, M.F., El-Sabban, H.A., Kang, J.H., El Shahawy, A., Alshwyeh, H.A., Hemdan, M., 2024. Exploring the sustainable synthesis pathway and comprehensive characterization of magnetic hybrid alumina nanoparticles phase (MHAl-NPsP) as highly efficient adsorbents and selective copper ions removal. *Environmental Technology & Innovation*, 34, P. 103628. https://doi.org/10.1016/j.eti.2024.103628

Rahman, I.N.A., Wahab, R.A., Mahat, N.A., Jamalis, J., Huri, M.A.M., Kurniawan, C., 2019. Ternary Blended Chitosan/Chitin/ FE 3O 4 Nanosupport for Lipase Activation and Stabilization. *Arabian Journal for Science and Engineering*, 44, pp. 6327–6337. https://doi.org/10.1007/s13369-019-03771-4

Ramírez, A., Sierra, L., Mesa, M., Restrepo, J., 2005. Simulation of nitrogen adsorption-desorption isotherms. Hysteresis as an effect of pore connectivity. *Chemical Engineering Science*, 60, pp. 4702–4708. https://doi.org/10.1016/j.ces.2005.03.004

Saad, R., Al-Bustan, 2005. Synthesis of Mesoporous Silica-based materials derivatized from Rice Husk and their Analytical Applications. Ph.D. Thesis. *University of Kerbala*, Kerbala, Iraq.

Saghapoor, Y., Alizadeh, R., 2021. A description of the proofs of formulas Langmuir, BET and Anderson related to adsorption isotherms-A Review. *Advanced Journal of Chemistry-Section B3*, pp. 62–67. https://doi.org/10.22034/ajcb.2021.118945.

Samiey, B., Cheng, C.H., Wu, J., 2014. Organic-inorganic hybrid polymers as adsorbents for removal of heavy metal ions from solutions: A review. *Materials*, 7, pp. 673–726. https://doi.org/10.3390/ma7020673

Simsek, E.B., Duranoglu, D., Beker, U., 2012. Heavy Metal Adsorption by Magnetic Hybrid-Sorbent: An Experimental and Theoretical Approach. *Separation Science and Technology*, 47, pp. 1334–1340. https://doi.org/10.1080/01496395.2012.672845

Song, Z.Z., Abula, A., Zhao, J.Y., Liu, G. Di, Li, M.R., Yang, D.L., Wang, Y.L., 2022. A novel hybrid thermodynamic model for pore size distribution characterisation for shale. *Petroleum Science*, 19, pp. 963–978. https://doi.org/10.1016/j.petsci.2021.12.015

Sugawara, E., Nikaido, H., 2014. Properties of AdeABC and AdeIJK efflux systems of Acinetobacter baumannii compared with those of the AcrAB-TolC system of Escherichia coli. Antimicrob. *Antimicrobial Agents and Chemotherapy*, 58, pp. 7250–7257. https://doi.org/10.1128/AAC.03728-14

Thommes, M., 2010. Physical adsorption characterization of nanoporous materials. *Chemie Ingenieur Technik*, 82, pp. 1059–1073. https://doi.org/10.1002/cite.201000064

Ugwu, E.I., Tursunov, O., Kodirov, D., Shaker, L.M., Al-Amiery, A.A., Yangibaeva, I., Shavkarov, F., 2020. Adsorption mechanisms for heavy metal removal using low cost adsorbents: A review. *IOP Conference Series: Earth and Environmental Science. IOP Publishing Ltd*, 614, P. 012166. https://doi.org/10.1088/1755-1315/614/1/012166

Verma, S., Jha, A.K., Shivam, S., Samanta, S.K., 2024. STUDIES ON ADSORPTION ISOTHERMS OF N2 ON BENTONITE. *Rasayan Journal of Chemistry,* 17, pp. 1340–1347. https://doi.org/10.31788/RJC.2024.1738784

Wang, S., Salim, O., Piri, M., 2025. The effects of pore shape and geometry on the storage of CO2 in mesoporous media. *Materials Today Sustainability*, 29, P. 101076. https://doi.org/10.1016/j.mtsust.2025.101076

Wilczyńska, A., Ruchomski, L., Łakomski, M., Góral-Kowalczyk, M., Surowiec, Z., Miaskowski, A., 2025. Chitosan-Coated Fe3O4 Nanoparticles for Magnetic Hyperthermia. *Materials,* 18, P. 5629. https://doi.org/10.3390/ma18245629

Wu, W., He, Q., Jiang, C., 2008. Magnetic iron oxide nanoparticles: Synthesis and surface functionalization strategies. *Nanoscale Research Letters*, 3, pp. 397–415. https://doi.org/10.1007/s11671-008-9174-9

Yu, H., Li, C., Yan, J., Ma, Y., Zhou, X., Yu, W., Kan, H., Meng, Q., Xie, R., Dong, P., 2023. A review on adsorption characteristics and influencing mechanism of heavy metals in farmland soil. *RSC Advances,* 13, pp. 3505–3519. https://doi.org/10.1039/d2ra07095b

Yu, S., Wang, J., Cui, J., 2020. Preparation of a novel chitosan-based magnetic adsorbent CTS@SnO_2@Fe_3O_4 for effective treatment of dye wastewater. *International Journal of Biological Macromolecules*, 156, pp. 1474–1482. https://doi.org/10.1016/j.ijbiomac.2019.11.194

Zhang, J., Lin, S., Han, M., Su, Q., Xia, L., Hui, Z., 2020. Adsorption properties of magnetic magnetite nanoparticle for coexistent Cr(VI) and Cu(II) in mixed solution. *Water*, 12, P. 446. https://doi.org/10.3390/w12020446

Zhang, M., Liu, Y., Yin, Z., Feng, D., Lv, H., 2023. Preparation and adsorption properties of magnetic chitosan/sludge biochar composites for removal of Cu^{2+} ions. *Scientific Reports*, 13, P. 20937. https://doi.org/10.1038/s41598-023-46815-4

Zhang, Z., Dong, W., Huang, Y., 2024. Oxidative degradation of chitosan by Fe-MCM-41 heterogeneous Fenton-like system. *Scientific Reports*, 14, P. 25972. https://doi.org/10.1038/s41598-024-76520-9

Zhao, F., Zhang, B., Feng, L., 2012. Preparation and magnetic properties of magnetite nanoparticles. *Materials Letters*, 68, pp. 112–114. https://doi.org/10.1016/j.matlet.2011.09.116

العلاقات بين البنية والنسيج في السيليكا المسامية الوظيفية بالكيتين منزوع الأسيتيل Fe_3O_4 كما كشفت عنها منحنيات امتزاز–إزالة امتزاز النيتروجين

تولين صلاح عثمان [1]، إقبال محمد مجتبى [2]، عمار صالح عباس [3]، *

[1] قسم الهندسة الكيميائية، كلية الهندسة، جامعة بغداد، بغداد، العراق

[2] قسم الصناعات الكيميائية، كلية البوليتكنيك – كركوك، جامعة التقنية الشمالية، كركوك، العراق

[3] قسم الهندسة الكيمياوية، كلية الهندسة، جامعة برادفورد، برادفورد ، المملكة المتحدة

الخلاصة

تناولت هذه الدراسة الخصائص النسيجية لثلاثة مواد ماصة باستخدام امتزاز/إزالة امتزاز النيتروجين عند درجة حرارة منخفضة ثابتة (77 كلفن). المواد الماصة هي: (أ) السيليكا المسامية المتوسطة (MS)، (ب) السيليكا المسامية المتوسطة المعدلة بأكسيد الحديد الثلاثي (MSF)، و(ج) السيليكا المسامية المتوسطة المعدلة بأكسيد الحديد الثلاثي والمغطاة بالكيتين منزوع الأسيتيل (MSFDAC). أظهر منحنى امتزاز/إزالة الامتزاز أن المواد الماصة المدروسة تمتلك بنية مسامية متوسطة من النوع الرابع، وفقًا لتصنيف الاتحاد الدولي للكيمياء البحتة والتطبيقية (IUPAC). تشير النتائج إلى أن منحنى بروناور–إيميت–تيلر (BET) يتوافق مع البيانات بشكل أفضل من منحنيي لانغمور وفروندليش. بلغت مساحة سطح MS أقصى قيمة لها مقارنةً بـ MSF وMSFDAC، والتي بلغت 1000.55 و168.05 و163.63 م²/غ على التوالي. أظهر تحليل توزيع حجم الجسيمات لجميع المواد الماصة نطاقًا ضيقًا، مما يشير إلى أن بنيتها مسامية متوسطة ومحددة جيدًا. على الرغم من وجود اختلافات طفيفة في توزيع قطر المسام نتيجةً لتحميل Fe_3O_4 والتعديل بالكيتين منزوع الأسيتيل، فإن مادة MSFDAC الماصة تُظهر عدم تجانس واختلافًا في أقطار الجسيمات. ازداد متوسط قطر المسام من MS (4.6 نانومتر) إلى MSF (7.32 نانومتر) ثم إلى MSFDAC (11.69 نانومتر). في المقابل، انخفض إجمالي حجم المسام من MS (1.15 سم³/غ) إلى MSF (0.89 سم³/غ) ثم إلى MSFDAC (0.48 سم³/غ). تم إجراء دراسة مقارنة مع الدراسات السابقة، والتي أظهرت أن الخصائص النصية للمادة الحيوية الماصة للسيليكا المغناطيسية المعدلة تتفق مع الدراسات الأخرى.

الكلمات المفتاحية: مركبات نانوية ذات بنية أساسية–غلافية، امتزاز الغازات الفيزيائي، تطور البنية المتوسطة، توزيع حجم المسام، نمذجة مساحة السطح.